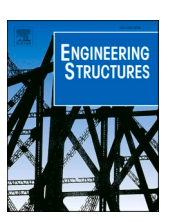
\$ SUPER

Contents lists available at ScienceDirect

Engineering Structures

journal homepage: www.elsevier.com/locate/engstruct





Hysteresis effect on earthquake risk assessment of moment resisting frame structures

Zhenhua Huang ^{a,*}, Liping Cai ^b, Yashica Pandey ^c, Yong Tao ^d, William Telone ^e

- ^a Department of Engineering Technology, University of North Texas, Denton, TX 76207, United States
- ^b Engineering College, University of North Texas, Denton, TX 76207, United States
- ^c College of Information, University of North Texas, Denton, TX 76207, United States
- d Interim Chair & BLG Endowed Professor, Department of Mechanical Engineering, Cleveland State University, Cleveland, OH 44115, United States
- e Department of Software and Information Systems, University of North Carolina at Charlotte, Charlotte, NC 28223, United States

ABSTRACT

It is essential to estimate the earthquake-induced risks of buildings. However, most popularly used earthquake fragility curves of moment-resisting frame buildings, such as the Hazards United States (HAZUS) Earthquake model, did not consider the effects of different hysteresis behaviors. This study aims at analyzing the hysteresis effects on the earthquake fragility curves of the Moment Resisting Frame Structures (MRFs) to extend applications of these curves. The SAC projected 3-story and 9-story MRF buildings were used in this study as examples. Hysteresis behaviors of the beam-column joint were used to describe the different behaviors of different types of National Earthquake Hazards Reduction Program (NEHRP) MRF structures. ELEMENT 10 in the DRAIN-2DX program was adopted to model these hysteresis behaviors of MRF joints. The fragility curves of 3-story and 9-story steel and RC MRF buildings with different hysteresis behavior models were successfully constructed using the cumulative lognormal distribution function. Based on these fragility curves, the seismic damage safeties of all MRF buildings with different hysteresis models and at different damage limit states were analyzed and compared. The results suggested that designers could utilize some reduction factors to conservatively design the structures when using the existing earthquake fragility analysis procedure for MRF structures, such as HAZUS, given the hysteresis behaviors of NEHRP MRF types. The earthquake fragility curves presented in this study could be directly adopted for the analysis of hysteresis behaviors of NEHRP MRF structures.

1. Introduction

To address the challenges of the damages of buildings and other civil infrastructures caused by hazards, civil engineers and researchers have developed many quantitative risk assessment methods for estimating or predicting the hazard-induced risks of buildings and other civil infrastructures. As an effective and reliable method to assess the possible building damages by hazards, the fragility curve method is a commonly accepted risk assessment procedure. To estimate the effect of the hazard on the damage probability level of buildings, fragility curves are developed to predict the probability of exceeding a threshold of the damage. To develop fragility curves for damage risk assessments, it is usually needed to determine the characteristic of probability distributions of the damaged status, such as the normal, lognormal, or uniform distributions. The lognormal distribution has been commonly accepted for residential building systems [17,16]. According to the curve categories [32], the fragility curves have four types, i.e., empirical, judgmental, analytical, and hybrid fragility curves. Rossetto and Elnashai [32] reported that empirical fragility curves are the most practical and reliable method for building risk assessment compared with the other three methods because they use real data. However, the method has drawbacks of highly specific to a particular situation and a specific type of building damages. Therefore, analytical fragility curves have been the most generated fragility curves. Initially developed by Veneziano et al. [43], the fragility curve for quantitative risk assessment of earthquake hazards was created in 1983. After that, the fragility curve method has been extended for the applications of other natural and non-natural hazards, such as tornados [24], hurricanes [41,14,18,26,2], flooding, tsunami [23,31,25], and fires [10].

The development of earthquake fragility curves needs to accurately estimate structure damages after seismic excitations and the quantification of ground motions. In practice, an earthquake fragility curve is commonly developed using the probability of the damage exceeding a critical threshold of a specified seismic intensity measure [47]. In their review paper, four different fragility analysis methods were discussed: (1) the safety factor method, (2) regression analysis; (3) maximum

E-mail addresses: zhenhua.huang@unt.edu (Z. Huang), Liping.Cai@unt.edu (L. Cai), YashicaPandey@my.unt.edu (Y. Pandey), y.tao19@csuohio.edu (Y. Tao), William.Tolone@uncc.edu (W. Telone).

^{*} Corresponding author.

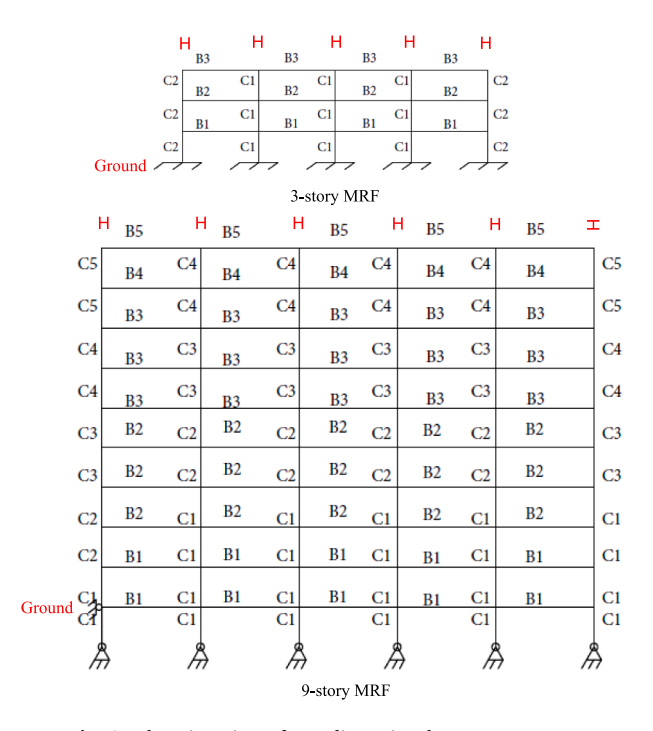


Fig. 1. Elevation view of two-dimensional MRF structures.

likelihood estimation from a set of nonlinear time history analysis; and (4) the incremental dynamic analysis method. These four fragility analysis methods were applied to determine fragility curves for the 3-story reinforced concrete shear wall building, in which, none of them

took the hysteresis effect into account. Monte Carlo method [28] and lognormal regression [20] are often used to evaluate the conditional probability. For example, Khalfan et al. [17] created empirical earthquake fragility curves by the lognormal regression, focusing on nonengineered residential buildings using shaking intensity maps in a geographic information system (GIS) format. In their work, the derived fragility curves were considered to be reasonable, the test of root mean square error (RMSE) indicated that the curves' predicts were within 7–17% of the actual probability of exceedance from the data, probably because the hysteresis effect was not counted in the calculation. Bao et al. [3] investigated the fragility of a structure that subjected to the impacts of earthquakes. A new method taking into account of the effect of post-shock damage was developed to generate earthquake analytical fragility curves. However, their work did not consider the hysteresis effect in their far-in fault and near-fault seismic sequences. More advanced statistical techniques have also been adopted to more efficiently conduct earthquake risk assessments using earthquake fragility curves, such as artificial neural networks (ANN) [27,4], support vector regression [11], etc. For example, an ANN method was utilized by Wang et al. [44] for improving the computational efficiency of fragility curves by implementing the delta method and verifying the validity of the lognormal distribution. The Federal Emergency Management Agency [9,8,7] published analytical tool of Hazards United States (HAZUS) [9,7], in which, the fragility curve method is utilized to conduct quantitative risk assessments for the damages resulted from hazards of tornados, hurricanes, earthquakes, and floods. The earthquake fragility curves in HAZUS have been extensively used by the governmental decision-makers to estimate potential losses by future earthquake hazards, which didn't consider the hysteresis effect as well.

As a popular building structural format, the moment-resisting frame (MRF) structure is usually assembled by rigidly connecting beams and columns. Fragility curves are often created to estimate the risk of MRF

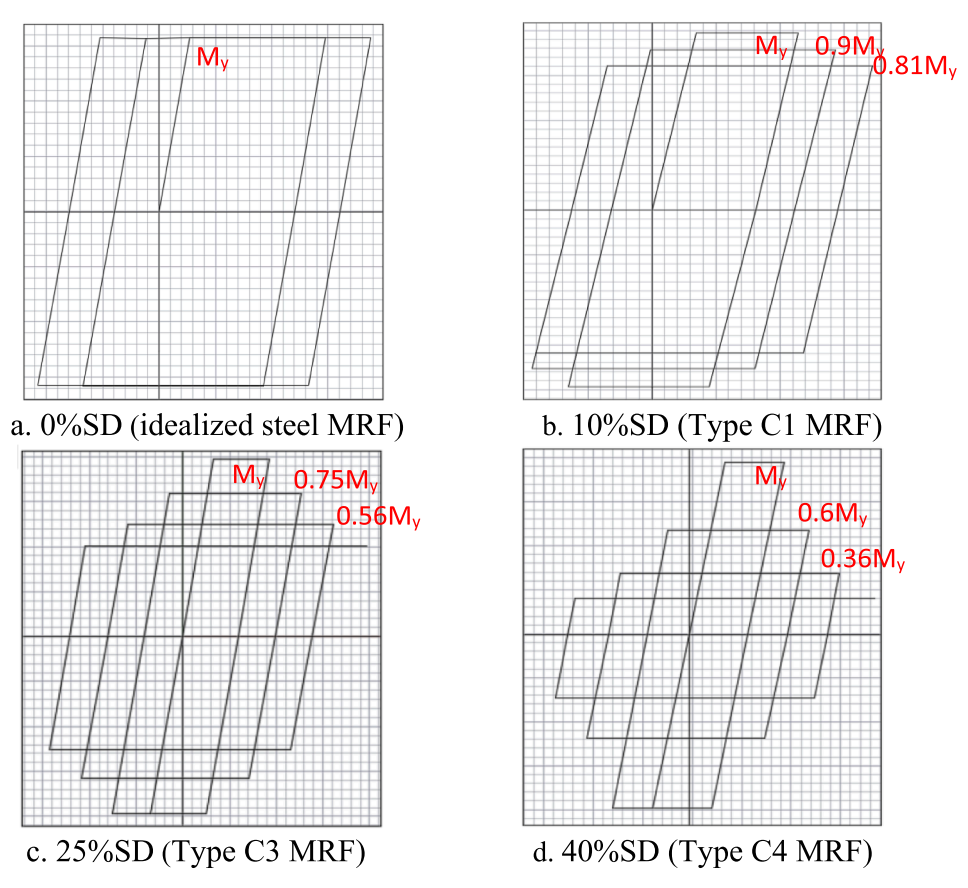


Fig. 2. Joint models of the NEHRP steel MRF structures.

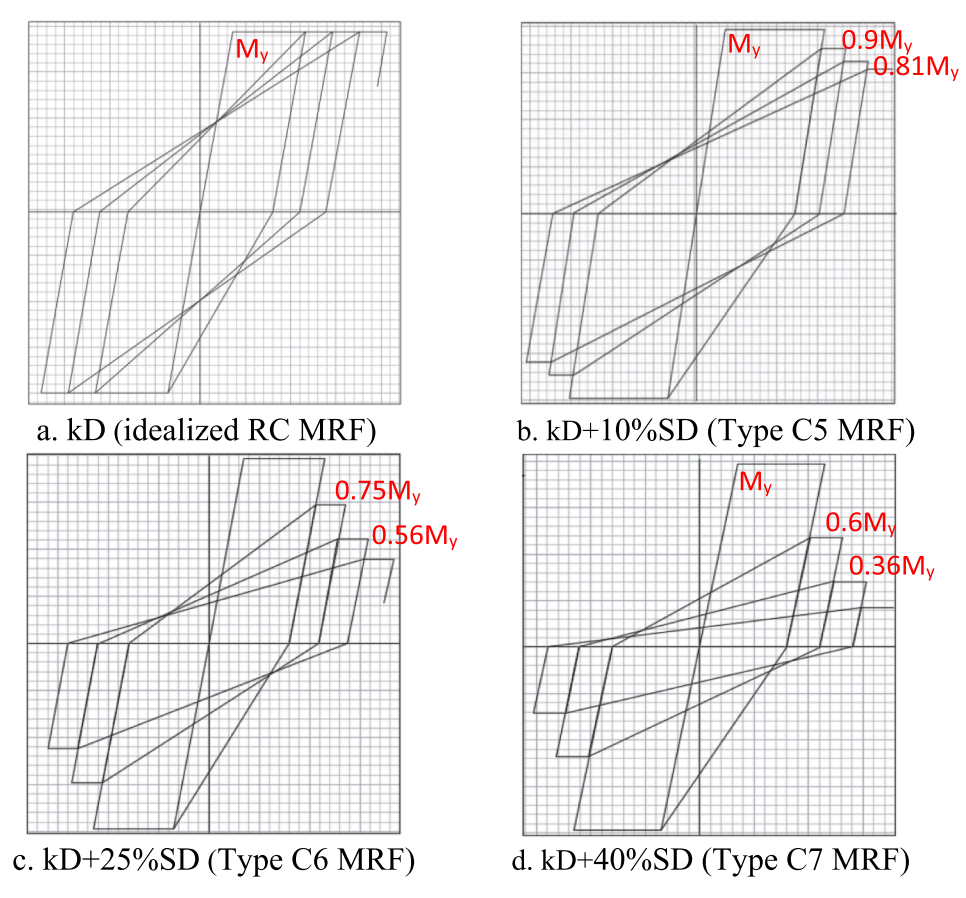


Fig. 3. Joint models of the NEHRP RC MRF structures.

structures attacked by earthquakes. Shafei et al. [35] utilized the collapse fragility database and pushover curves to develop closed-form equations. Using the parallel fragility computing method, the collapse margin ratios of MRF structures were calculated by Hardyniec and Charney [13]. The effect of inherent uncertainties on the performance of MRFs during the earthquake was investigated by Asgarian and Ordoubadi [1] using the fragility analysis of seismicity. By considering capacity limits, seismic fragility curves of MRFs with magnetorheological dampers were created by Cha and Bai [5].

Modern codes, such as FEMA 355F and 2009 NEHRP, proposed three types of steel MRF and three types of reinforced concrete (RC) MRF with different earthquake resistance capacities. They include Type C1 - Special Steel MRF, Type C3 - Intermediate Steel MRF, Type C4 - Ordinary Steel MRF, Type C5 - Special RC MRF, Type C6 - Intermediate RC MRF, and Type C7 - Ordinary RC MRF. Different types of MRFs have different earthquake damage fragilities. A numerical example in Yun et al. [45] investigated the performance of steel MRF during earthquakes and proposed the relationships between the probability and prevention performance level. Huang and Foutch [15] proposed the use of the hysteresis behaviors of the beam-column joints to model the performance of the different types of NEHRP MRFs. Hysteresis behavior is the lagging of the deformation of the building component after an earthquake. After the earthquake, the component either immediately springs back to its original state or somehow changes from previous deformations. However, Huang and Foutch didn't explore the hysteresis effects on fragility curves.

In summary, the literature review indicated that all reports regarding the fragility analyses of MRFs did not consider hysteresis effects during earthquakes. Studies discussed hysteresis behaviors of MRF during earthquakes, such as Huang and Foutch [15], did not perform fragility analyses. Thus, this present study initially proposed fragility curves with consideration of hysteresis effect and provided designers with reduction

factors, which can be directly utilized to the practical NEHRP MRF structure design. The contributions of this research can be summarized as follows:

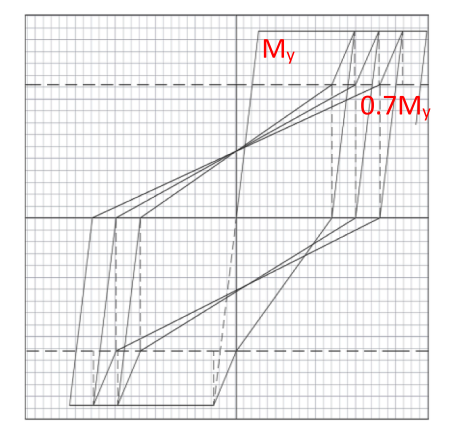
- (1) Explored the effects of hysteresis behaviors on earthquake fragility curves of moment-resisting frame structures.
- (2) Developed a group of earthquake fragility curves with consideration of hysteresis effects, which can be applied to designs of different NEHRP MRF structures and served as a measure of assessing structure vulnerability, providing decision-makers with a better understanding of structural behavior when an earthquake occurs.
- (3) Provided a group of hysteresis behavior reduction factors that can be used for building design when designers and decision-makers adopting other existing earthquake fragility curves for MRF structures, such as the HAZUS model.

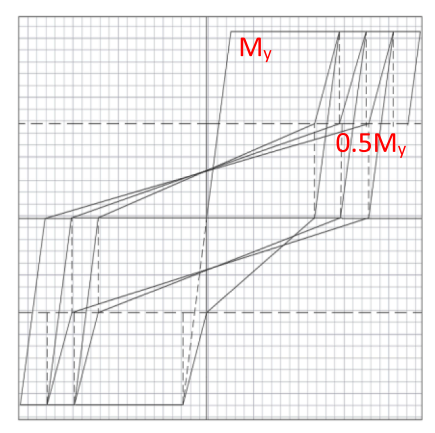
2. Case study of moment resistance frame structures

The buildings in this study were the SAC project prototype buildings with 3-story and 9-story steel MRF structures [46]. Elevation views of two-dimensional MRF structures of this study are presented in Fig. 1.

For the 3-story building, there is no basement and no concrete wall anywhere. It is assumed that bay spans are 30 feet (total four spans of MRFs), and column heights are 13 feet. All beams and columns are bending about their strong axes. To prevent bi-axial bending, no corner column is employed for the MRF.

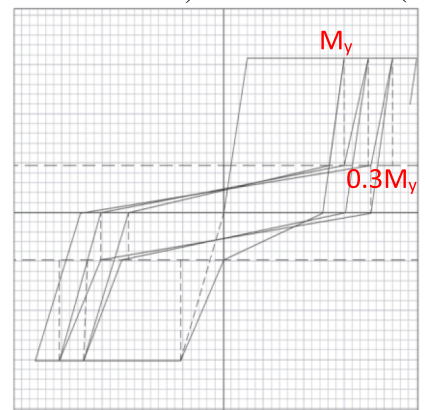
For the 9-story building, there is one basement and concrete walls are used to prevent the lateral movement at the ground floor level, which was modeled by restraining the ground floor. Bay spans of the MRF are 30 feet with a total of 4-1/2 spans. This means that 4 spans of the MRF have moment connections with beams connected to the strong bending





70% Pinch (short slip or small crack)

50% Pinch (medium slip or crack)



30% Pinch (long slip or large crack)

Fig. 4. Joint models of the NEHRP MRF structures with different bolt slippery distances for steel MRF structures and different crack dimensions for RC MRF structures.

Table 1
3-story moment-resisting frame configuration.

| Member | Steel Member | Stiffness EI (x10 ⁶ k-in ²) |
|--------|--------------|--|
| C1 | W14x283 | 111 |
| C2 | W14x257 | 99 |
| B1 | W27x114 | 118 |
| B2 | W27x102 | 105 |
| B3 | W18x50 | 23 |

Table 29-story moment-resisting frame configuration.

| 9-story moment-resisting frame configuration. | | | | | |
|---|--------------|--|--|--|--|
| Member | Steel Member | Stiffness EI (x10 ⁶ k-in ²) | | | |
| C1 | W14x500 | 238 | | | |
| C2 | W14x455 | 209 | | | |
| C3 | W14x398 | 174 | | | |
| C4 | W14x283 | 111 | | | |
| C5 | W14x257 | 99 | | | |
| B1 | W36x150 | 262 | | | |
| B2 | W33x141 | 216 | | | |
| В3 | W30x116 | 143 | | | |
| B4 | W24x94 | 78 | | | |
| B5 | W18x60 | 29 | | | |

direction (x-x direction) of columns and one extra span of the MRF has moment connections with beams connected to the weak bending direction of columns. All columns have a height of 13 feet, as well. To avoid bi-axial weak axis bending, only one moment-connection was designed for each corner column. Columns were pin-supported at the

Table 3Mapping of NEHRP MRF structures and hysteresis models.

| Frames Type | Frame Description | Hysteresis Model | Model Demo |
|----------------|--------------------------|------------------|---------------|
| NEHRP Stee | l MRF | | |
| | Ideal steel MRF | 0% SD | Fig. 2a |
| Type C1 | Special steel MRF | 10%SD | Fig. 2b |
| Type C3 | Intermediate steel MRF | 25%SD | Fig. 2c |
| Type C4 | Ordinary steel MRF | 40%SD | Fig. 2d |
| Slip | Bolt connection slippage | 30, 50, 70% | Fig. 4 |
| | | Pinching | |
| NEHRP RC | MRF | | |
| | Ideal RC MRF | kD | Fig. 3a |
| Type C5 | Special RC MRF | kD + 10%SD | Fig. 3b |
| Type C6 | Intermediate RC MRF | kD + 25%SD | Fig. 3c |
| Type C7 | Ordinary RC MRF | Kd + 40%SD | Fig. 3d |
| Cracked | Opening/closing of the | 30, 50, 70% | Fig. 4 |
| | cracks | Pinching | |

basement level

Member dimensions for the 3-story and 9-story buildings are shown in Tables 1 and 2, respectively. The strength and stiffness of these buildings represented current steel MRF buildings being constructed today. RC MRF buildings with the same heights and similar plan configurations would likely be heavier and stiffer but have similar periods (natural frequencies) as these steel MRF buildings. Therefore, the readers should not consider this to be a study of steel MRF buildings. The material should be thought of as generic. Hysteresis properties were changed to represent hysteresis behaviors of both steel and reinforced concrete frames.

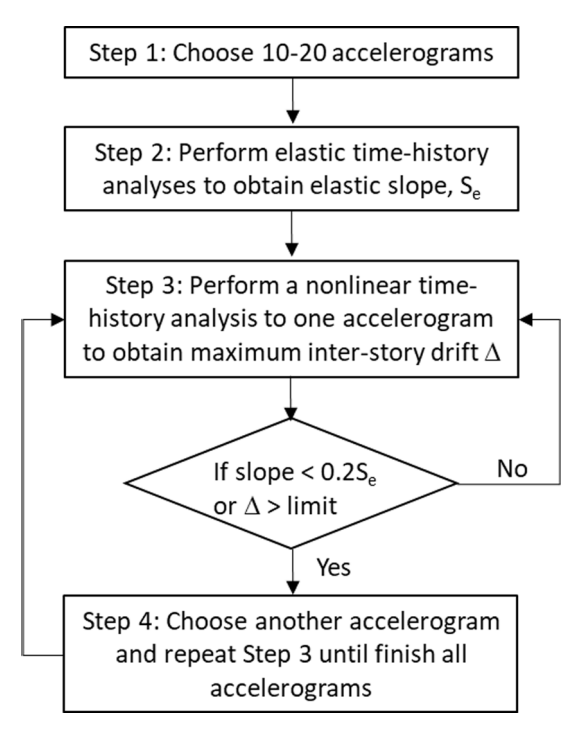


Fig. 5. Flowchart for Incremental Dynamic Analysis (IDA).

Table 4Ground motions for IDA.

| No. | M | Year | Name | PGA (cm/s ²) | Duration (sec) |
|-----|-----|------------|-----------------------|--------------------------|----------------|
| 1 | 7.1 | 1992 | Mendocino X | 741.13 | 59.98 |
| 2 | 7.1 | 1992 | Mendocino Y | 476.22 | 59.98 |
| 3 | 6.7 | 1992 | Erzincan X | 593.6 | 20.775 |
| 4 | 6.7 | 1992 | Erzincan Y | 529.06 | 20.775 |
| 5 | 6.5 | 1949 | Olympia X | 878.23 | 79.98 |
| 6 | 6.5 | 1949 | Olympia Y | 805.68 | 79.98 |
| 7 | 7.1 | 1965 | Seattle X | 1722.4 | 81.82 |
| 8 | 7.1 | 1965 | Seattle Y | 1364.7 | 81.82 |
| 9 | 8 | 1985 | Valpariso X | 1605.5 | 99.975 |
| 10 | 8 | 1985 | Valpariso Y | 1543.5 | 99.975 |
| 11 | 7.9 | simulation | Deep Inter-plate 1 | 781.31 | 79.98 |
| 12 | 7.9 | simulation | Deep Inter-plate 2 | 634.36 | 79.98 |
| 13 | 7.9 | simulation | Shallow Inter-plate 1 | 524.55 | 79.98 |
| 14 | 7.9 | simulation | Shallow Inter-plate 2 | 567.18 | 79.98 |
| 15 | 7.9 | simulation | Shallow Inter-plate 3 | 735.22 | 79.98 |

In this study, hysteresis types considered consist of that for buildings with modern well-detailed steel and RC frames, and with moderate and non-ductile steel and/or RC constructions. This study focuses on those buildings that have strong columns and weak beams; therefore, the first yielding can always occur at components of beams.

3. Analytical modelling of MRF

The software of DRAIN-2DX [30] was selected to model steel and RC MRF structures in this study and to conduct nonlinear dynamic analyses because it can model different and complicated hysteresis behaviors of beam-to-column joints.

The nonlinear centerline model with rotational springs of DRAIN-2DX was used to analyze MRF behaviors in this study, in which the panel zone effects were not considered. The elastic elements connected by the joints were utilized to simulate beams. The rotational springs were placed at the end of beam elements, being used to simulate the inelastic behavior of beams. Due to the full rigid connection behavior of rotational springs, the initial elastic stiffness was large, being assigned as $k=6\times 10^6\ k\text{-in}$. Thus, the initial stiffness of the frame can be provided by beam elements because of their elastic behavior. When the plastic

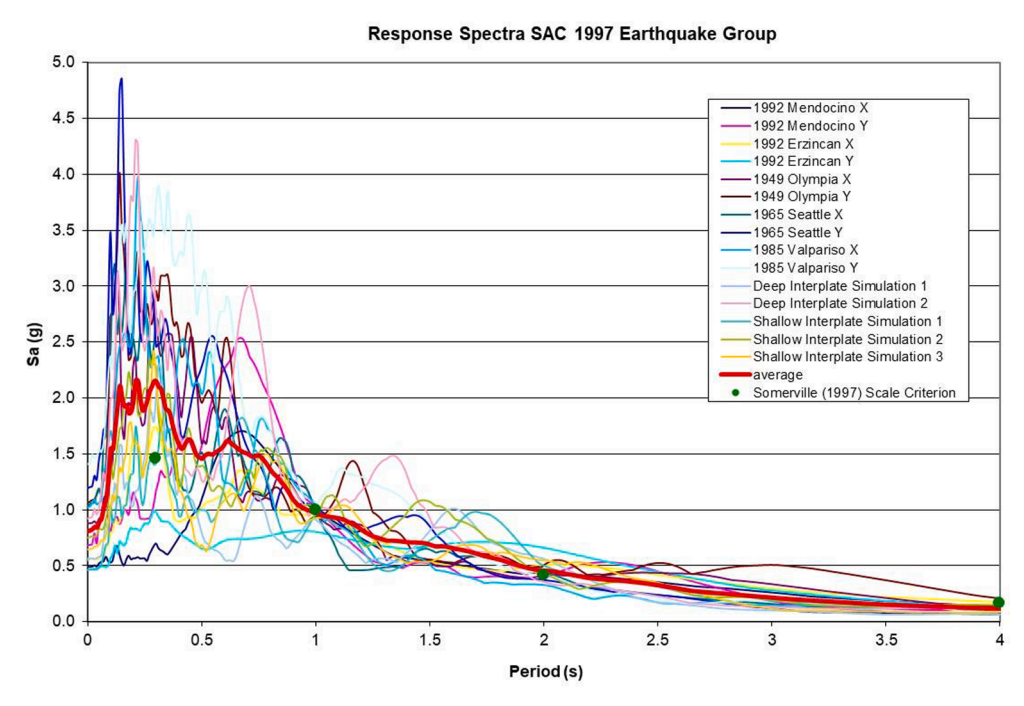


Fig. 6. Response Spectra of the 15 selected earthquake records scaled by Somerville [39].

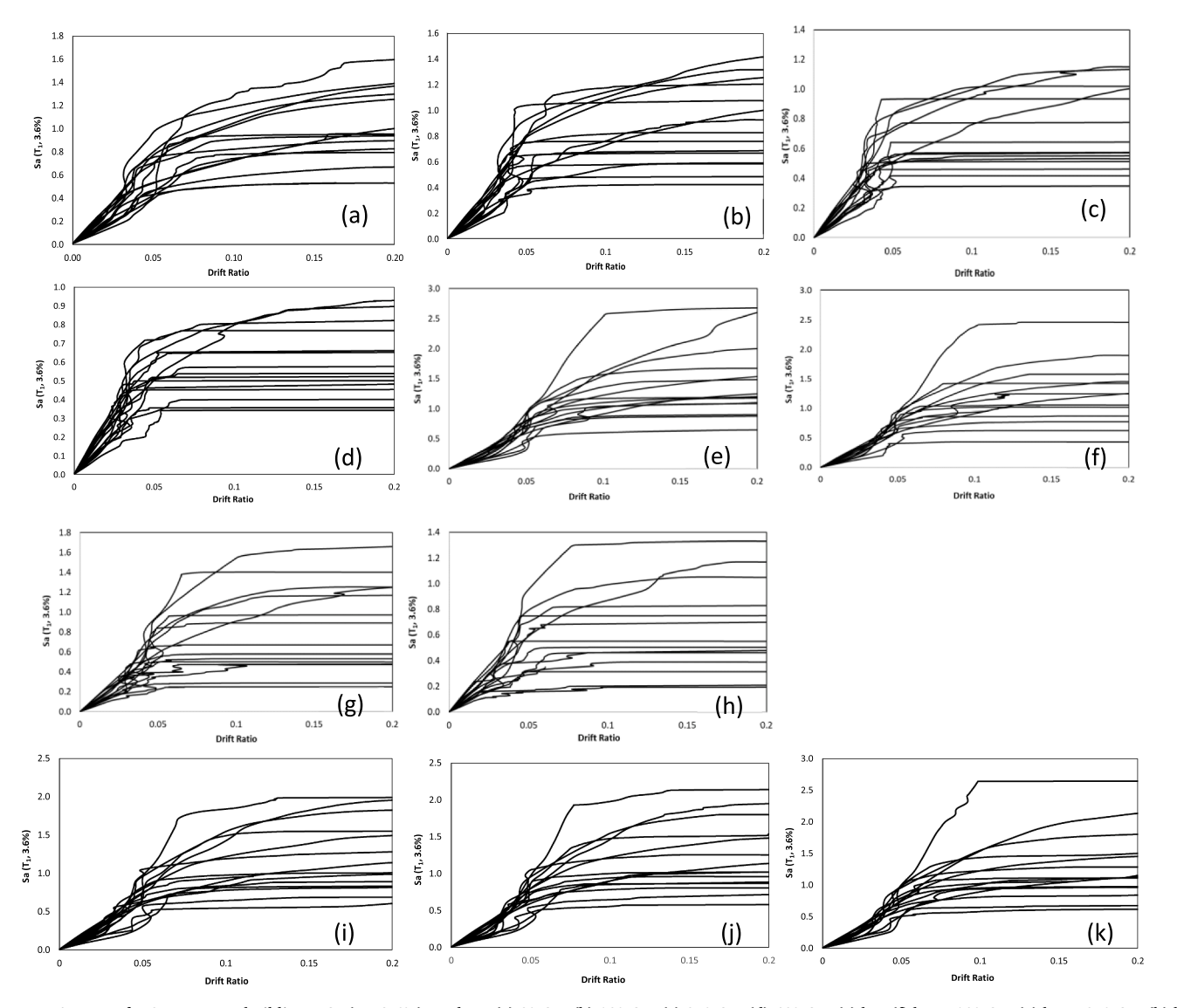


Fig. 7. IDA curves for 9-story MRF buildings - Sa (T_1 , 3.6%) vs. d_{max} : (a) 0%SD, (b) 10%SD, (c) 25%SD, (d) 40%SD, (e) kD, (f) kD + 10%SD, (g) kD + 25%SD, (h) kD + 40%SD, (i) 30%Pinch, (j) 50%Pinch, (k) 70%Pinch.

Table 5Significance values of log-normality tests and means and standard deviations.

| Туре | Damage state | Sample size | Kolmogorov-Smirnov* | Shapiro-Wilk | | Log Std Deviation | Correlation R ² |
|--------------------|--------------|-------------|---------------------|--------------|--------|-------------------|----------------------------|
| | | | | • | Median | | |
| Ideal steel | Minor | 15 | 0.181 | 0.133 | 0.590 | 0.174 | 0.9264 |
| | Medium | 15 | 0.200** | 0.794 | 0.854 | 0.241 | 0.9257 |
| | Severe | 15 | 0.200 | 0.299 | 0.968 | 0.292 | 0.9254 |
| | Collapse | 15 | 0.200 | 0.561 | 1.016 | 0.328 | 0.9254 |
| Special steel | Minor | 15 | 0.200 | 0.415 | 0.643 | 0.206 | 0.9259 |
| - | Medium | 15 | 0.184 | 0.203 | 0.793 | 0.251 | 0.9258 |
| | Severe | 15 | 0.200 | 0.340 | 0.849 | 0.290 | 0.9257 |
| | Collapse | 15 | 0.200 | 0.514 | 0.876 | 0.318 | 0.9258 |
| Intermediate steel | Minor | 15 | 0.131 | 0.396 | 0.596 | 0.177 | 0.9260 |
| | Medium | 15 | 0.174 | 0.170 | 0.664 | 0.225 | 0.9260 |
| | Severe | 15 | 0.091 | 0.156 | 0.690 | 0.257 | 0.9262 |
| | Collapse | 15 | 0.200 | 0.196 | 0.714 | 0.271 | 0.9260 |
| Ordinary steel | Minor | 15 | 0.200 | 0.570 | 0.516 | 0.129 | 0.9253 |
| | Medium | 15 | 0.200 | 0.180 | 0.586 | 0.167 | 0.9259 |
| | Severe | 15 | 0.200 | 0.199 | 0.601 | 0.188 | 0.9261 |
| | Collapse | 15 | 0.200 | 0.235 | 0.605 | 0.196 | 0.9262 |

^{*} Lilliefors Significance Correction [21].

^{**} This is a lower bound of the true significance.

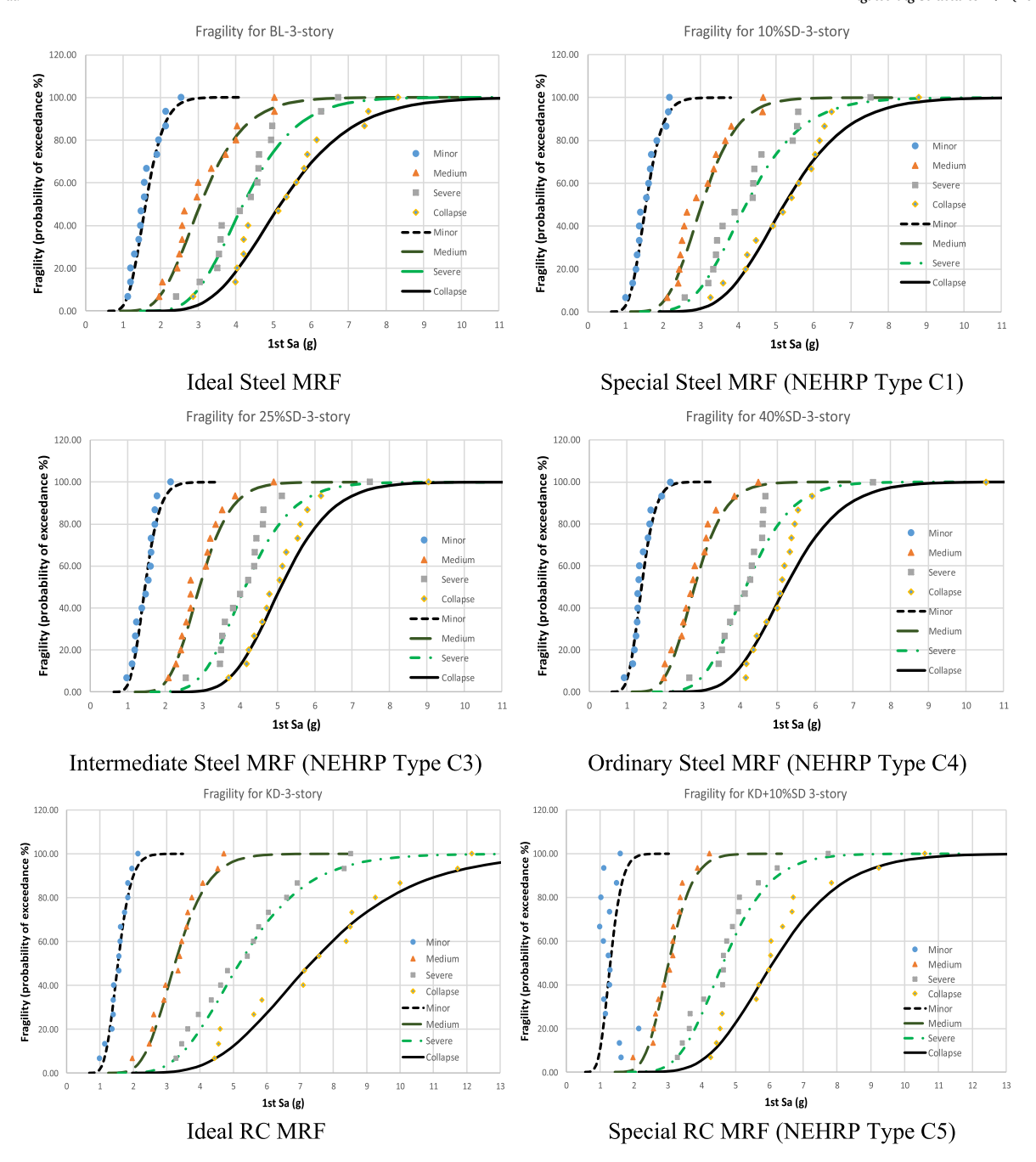
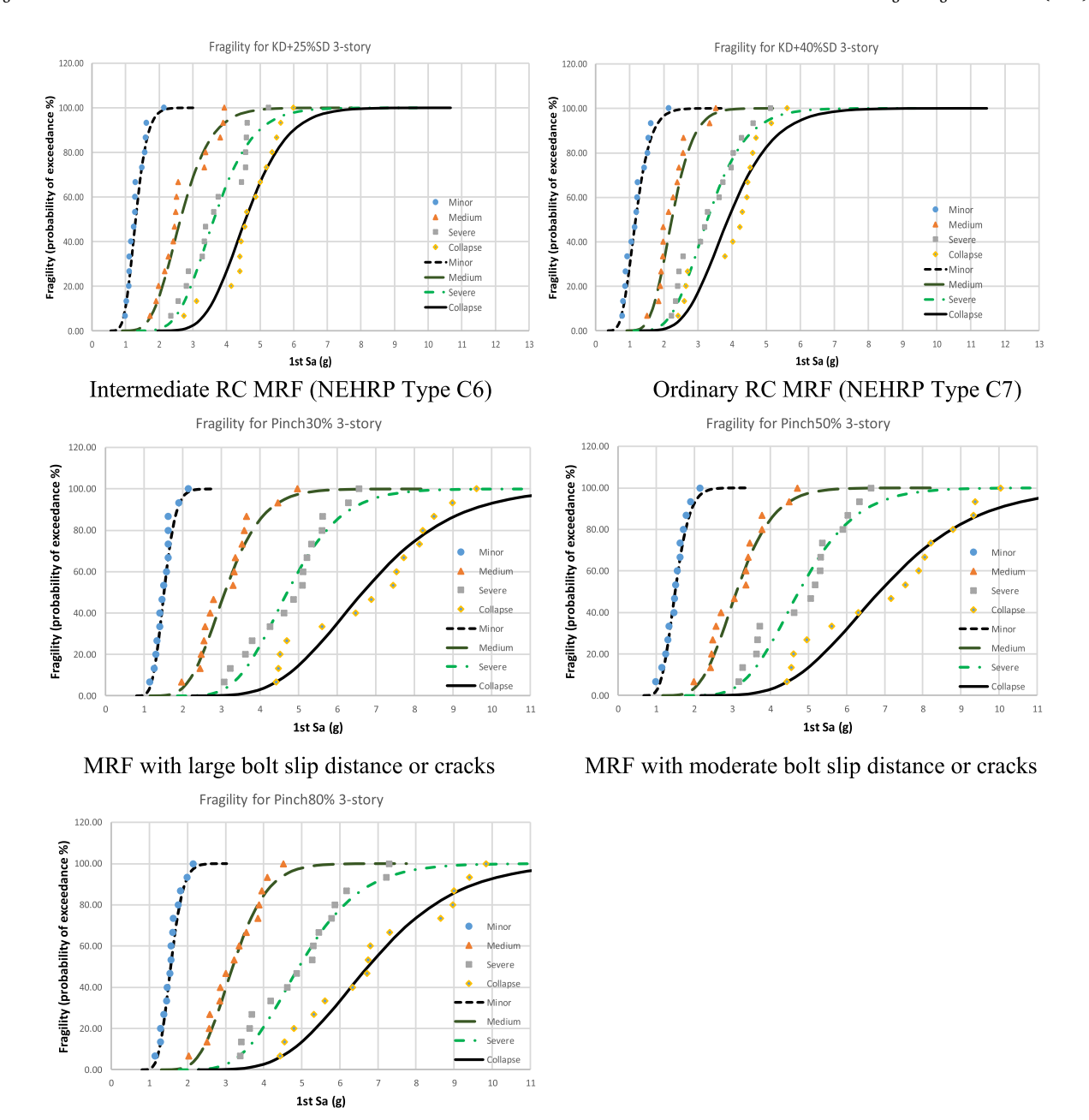


Fig. 8. Fragility Curves of 3-story Steel and RC Moment Resisting Frame Buildings.

moment capacity was reached, the strain-hardening rate was assumed 0.3% for the post-yield stiffness of the rotational spring. Using the DRAIN-2DX program, columns were considered as the beam-column elements. By considering the geometry nonlinearity, the P- Δ and P- δ effects were considered when conducting the nonlinear time-history analyses. The P- Δ effects were calculated by applying a load combination with 100% dead load and 25% live load on the frame elements and leaning columns. During the dynamic time-history analyses, the 4.3% damping was used for the 3-story building simulation, while 3.6% was used for the 9-story building simulation because these damping values have been recommended for the instrumented MRF buildings during earthquakes [12]. During the simulation, these damping values were assigned to the first and second modes.

Hysteresis behaviors of the beam-column joint are important

characteristics of MRF structures. The joint hysteretic behaviors include stiffness degradation (kD), strength degradation (SD), and pinching. SD is a typical hysteresis behavior of steel MRF joints. Due to the local buckling of steel beams, the joint strength could be reduced somewhat after each execution of yielding. The strength loss rate for each cycle is a function of the flange slenderness ration $b_t/2t_f$ of the steel beam element and the maximum rotation θ_{max} of previous cycles [45]. The kD model in accordance with the Takeda-Sozen model [42] represents the hysteresis behavior of the ideal RC MRF joints. This model was considered as an ideal theoretical model that cannot be used for simulating the behavior of an actual RC MRF building because the SD behavior inevitably occurs together with the kD behavior at large story drifts during vibrations. Using the kD model, according to different periods of cracking, yielding, and loading/unloading during the loading cycles, the stiffness



MRF with small bolt slip distance or cracks

Fig. 8. (continued).

parameters of RC MRF structures were specified. Since the kD model is a peak oriented, the direction of the reloading stiffness degrades is developed towards the direction of the previous max peak point of the loading. According to the reports by LaFave and Wight [19] and Shin and LaFave [37], as one of the important properties for a hysteresis behavior, the pinching of the hysteresis loop can be caused by the opening/closing of the cracks and/or the slipping of debonded reinforcing bars in RC structures, which is needed to be explored. According to the article by Schneider and Teeraparbwong [34], the bolt connection slippage under loading reversal in steel structures also caused pinching. Shi and Foutch [36] developed a new element (ELEMENT 10) in the software of DRAIN-2DX, which can model these hysteresis behaviors of the MRF joints. Base on the report of Huang and Foutch [15], Table 3 shows the mapping of NEHRP MRF structures and different hysteresis models.

4. IDA analysis

Luco and Cornell [22] developed a method to analyze the hysteresis effect on earthquake risk assessment using the incremental dynamic analysis (IDA) procedure, being employed to develop data needed for creating fragility curves. Described in FEMA355f, the IDA procedure shown in Fig. 5 can be used to study the relationship between the intensity measure (IM) of ground motion and the engineering demand parameter (EDP) up to collapse during an earthquake. The IDA framework can be described as that the response history analysis of structures is executed according to the increasingly scaled historical earthquake data. IM and EDP are usually considered as peak ground acceleration (PGA) or approximately 5% damped fundamental spectral acceleration, Sa (T_1 , 5%), and the max inter-story drift ratio, d_{max} , respectively [6].

In this study, the IM was taken as the 4.3% damped fundamental spectral acceleration Sa $(T_1, 4.3\%)$ for the 3-story MRF buildings and

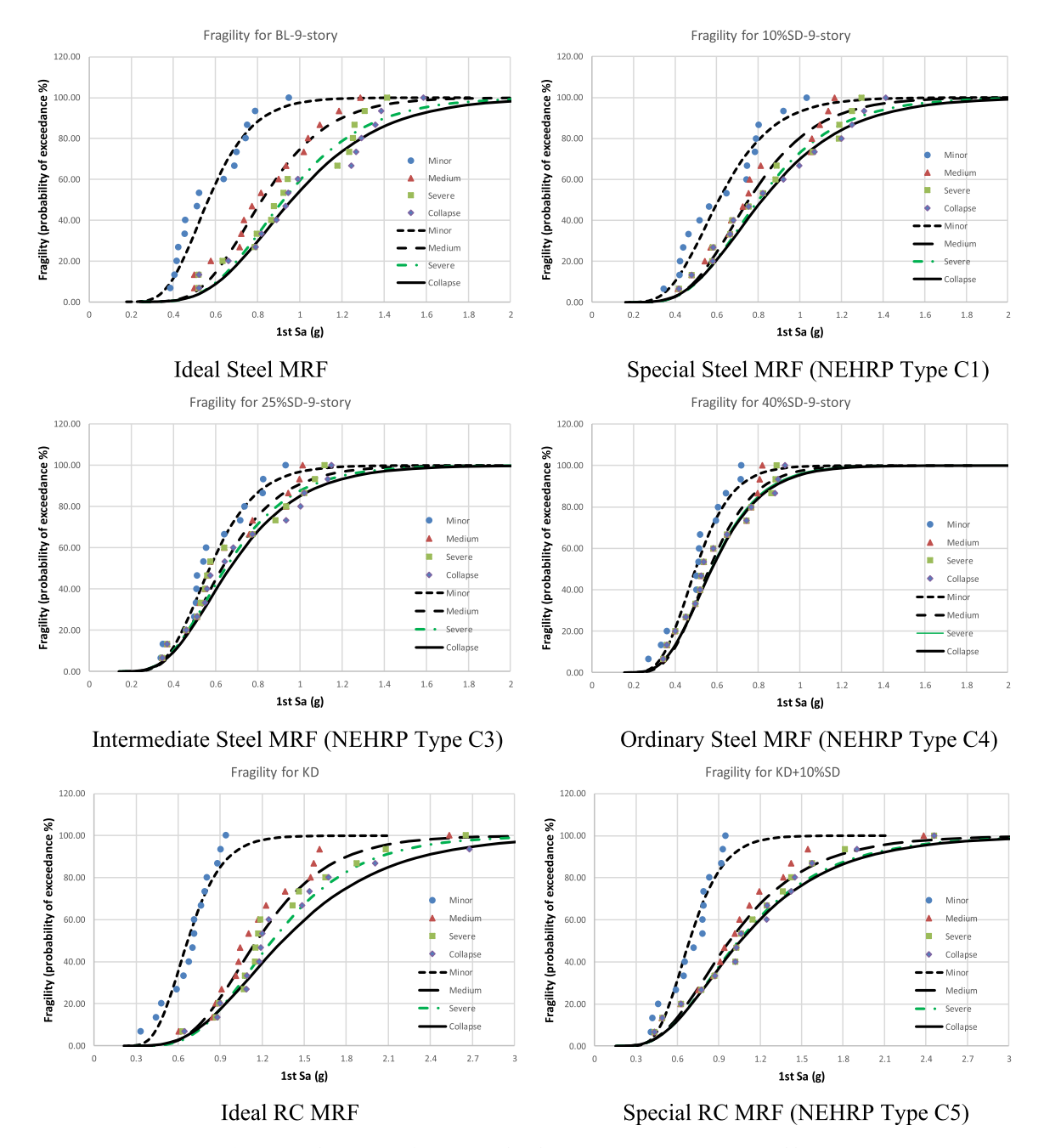


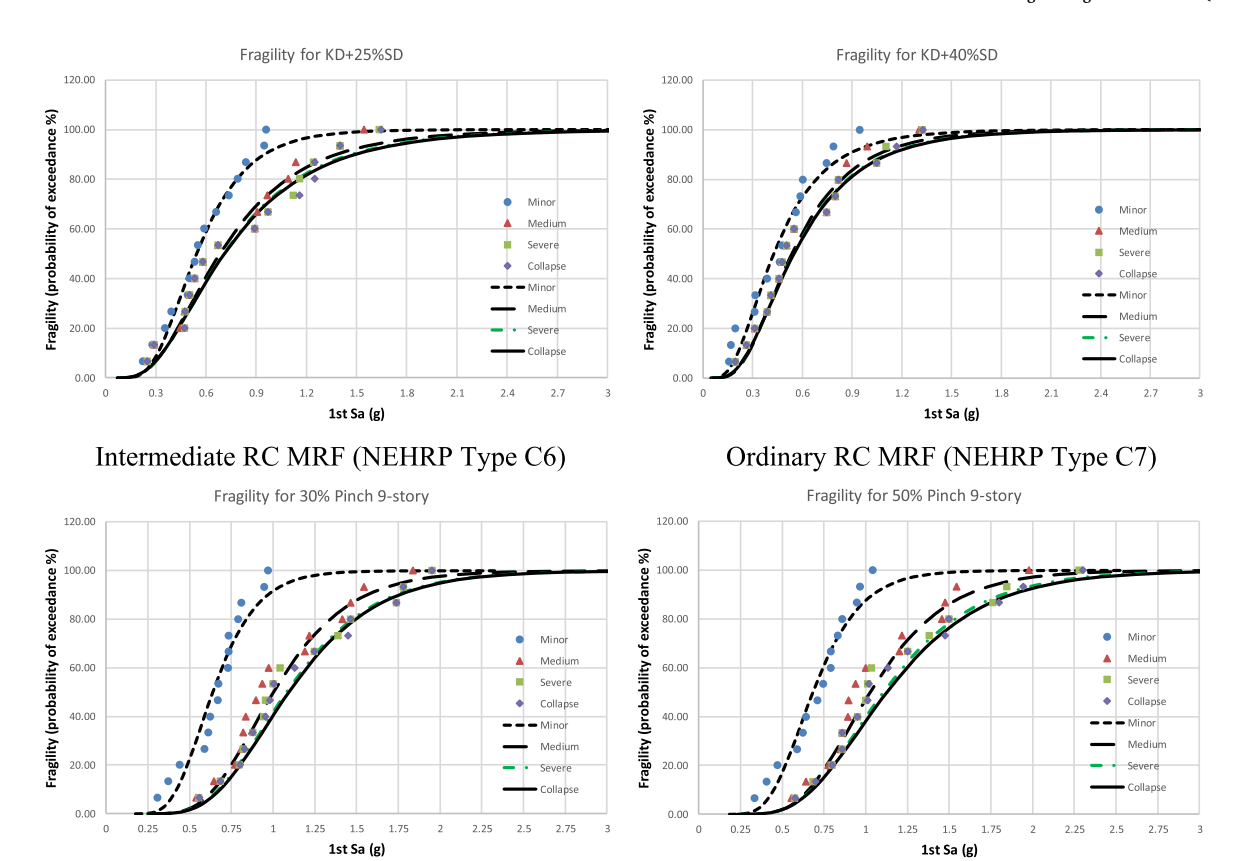
Fig. 9. Fragility Curves of 9-story Steel and RC Moment Resisting Frame Buildings.

3.6% damped fundamental spectral acceleration Sa $(T_1, 3.6\%)$ for the 9-story MRF buildings. The EDP was taken as the max inter-story drift ratio, d_{max} . Table 4 shows that fifteen ground motions from the SAC project, SAC-96-02 [33], were selected for the IDA to consider the uncertainty of earthquakes. Fig. 6 shows the response spectra of the fifteen ground motions using the Somerville [39] scaling criterion. The resulted IDA curves for 9-story steel and RC MRF buildings with different hysteresis models are shown in Fig. 7.

5. Earthquake fragility curves

Earthquake fragility is the probability of exceeding a defined damage limit state of a structure with an intensity measure of ground movement. The present study utilized a mathematical method to develop the earthquake fragility curves using the method of IDA. As discussed in the

previous section, the 4.3% and 3.6% damped spectral accelerations at fundamental periods of Sa (T_1 , 4.3%) and Sa (T_1 , 3.6%) were adopted as the earthquake intensity measure for the MRF buildings of 3-story and 9-story, respectively. Based on the analysis in Huang and Foutch [15], the maximum cutoff drift limit for the global collapse limit state was set at 0.20 or the slope of IDA curves decreased to a value smaller than 0.2 of the median of their initial slope. According to the IDA curves in Fig. 7, the global minor damage limit state was set as 0.05 to simulate global 'yielding' points on these IDA curves. Then, 0.10 and 0.15 were manually picked as the two intermediate damage limit states (medium and severe) between the global minor and global collapse limit states. The analytical model for selected drift limits would not be realistic because local collapses and shambles of building contents would likely occur prior to this and/or the mathematical model would no longer be valid. However, the selected global limit states worked for this study because



MRF with large bolt slip distance or cracks

Fragility for 80% Pinch 9-story

120.00

100.00

Minor

Medium

Severe

Collapse

On 0.25 0.5 0.75 1 1.25 1.5 1.75 2 2.25 2.5 2.75 3

MRF with small bolt slip distance or cracks

Fig. 9. (continued).

the purpose of this study is to investigate the effects of hysteresis behavior on global collapses.

This study used the lognormal probability distribution function for describing the fragility performance because it is the most popular model used for earthquake risk assessments currently [29]. The cumulative lognormal distribution function can be written as

$$F_x(D \ge d_j|w_i) = \varnothing\left(\frac{\ln p_i - \mu_i}{\sigma_i}\right) \tag{1}$$

where, F_x is the probability of a damage limit state; D is a damage limit state equal to or greater than the j^{th} damage limit state, d_j , given the damped spectrum acceleration for the fundamental period, Sa $(T_1, -\%)$, w_i is the damage state number; $\Phi(*)$ is the function of normal CFD, p_i is the random variate, namely, the air-blast incident overpressure (kPa), μ_i is the logarithmic mean and σ_i is the logarithmic standard deviation of

the i^{th} damage limit state. Eq. (1) can be written as:

MRF with moderate bolt slip distance or crack

$$F_x(D \ge d_j | w_i) = \frac{1}{2} \left[1 + erf\left(\frac{\ln(p) - \mu}{\sigma\sqrt{2}}\right) \right]$$
 (2)

where *erf* is the Gauss error function. There could be associated threshold levels for a given Sa $(T_1, -\%)$, resulting in separate fragility curves for specific damage limit states. Then, the fragility curve with a random number could be used to evaluate whether damage occurs for a given Sa $(T_1, -\%)$, depending on whether the random number is greater than the fragility value for that Sa $(T_1, -\%)$.

To confirm that if the function of the cumulative lognormal distribution is suitable for presenting the fragility relationships between the probability of exceeding a specific damage limit state and the damped fundamental spectral acceleration Sa $(T_1, -\%)$, the statistic software SPSS (IBM SPSS 25) was utilized for testing the performance of the log-

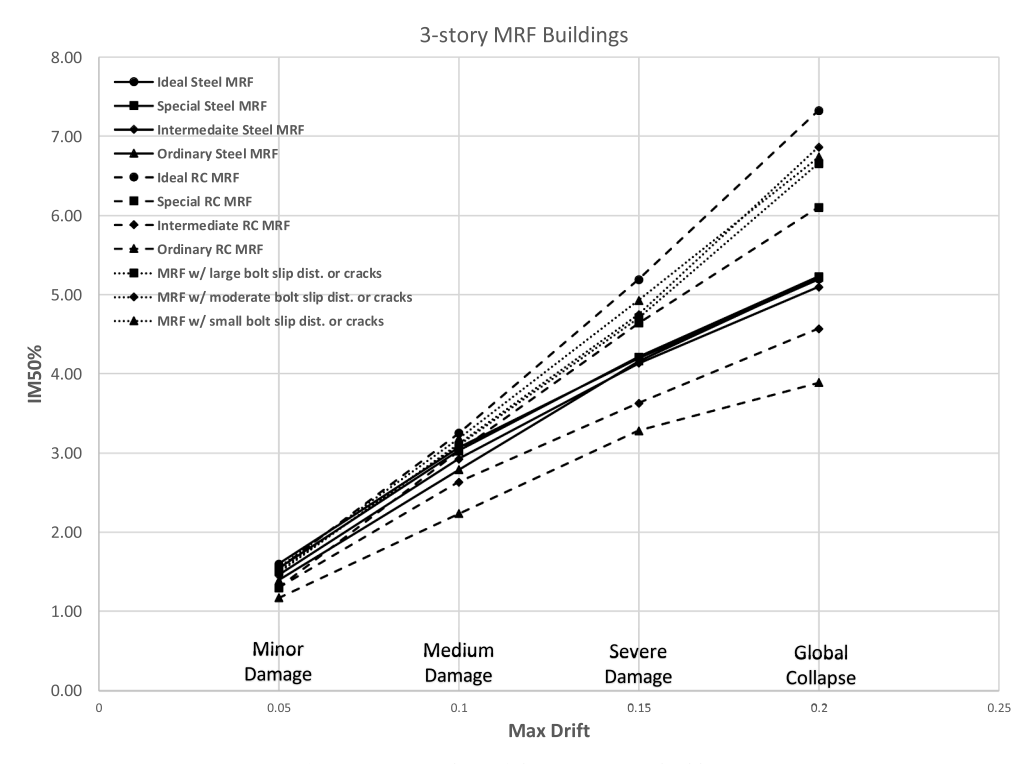


Fig. 10. $IM_{50\%}$ values of the 3-story MRF buildings.

normality of the distributions. The Kolmogorov-Smirnov test (KS) [21] and the Shapiro-Wilk (SW) test were utilized to check if the data belong to the lognormal distribution. The Hypothesis was that the distribution of determined data is Not significantly different from a lognormal distribution at a significant level of $\alpha=0.05$.

As an example, data of the 9-story steel MRF building with no SD model (idealized 9-story steel MRF) was utilized for the normality tests. The test results are presented in Table 5. Because all the KS and SW

Significance values in Table 5 are greater than $\alpha=0.05$, the hypothesis was proved as 'accepted'. Both the KS and SW tests are the nonparametric tests of the equality of continuous probability distributions that can be used to compare a sample with a reference probability distribution, which can serve for the goodness of fit tests. In the case of testing for lognormality of the distribution, samples are standardized and compared with a standard lognormal distribution. This is equivalent to setting the median and variance of the reference distribution equal to

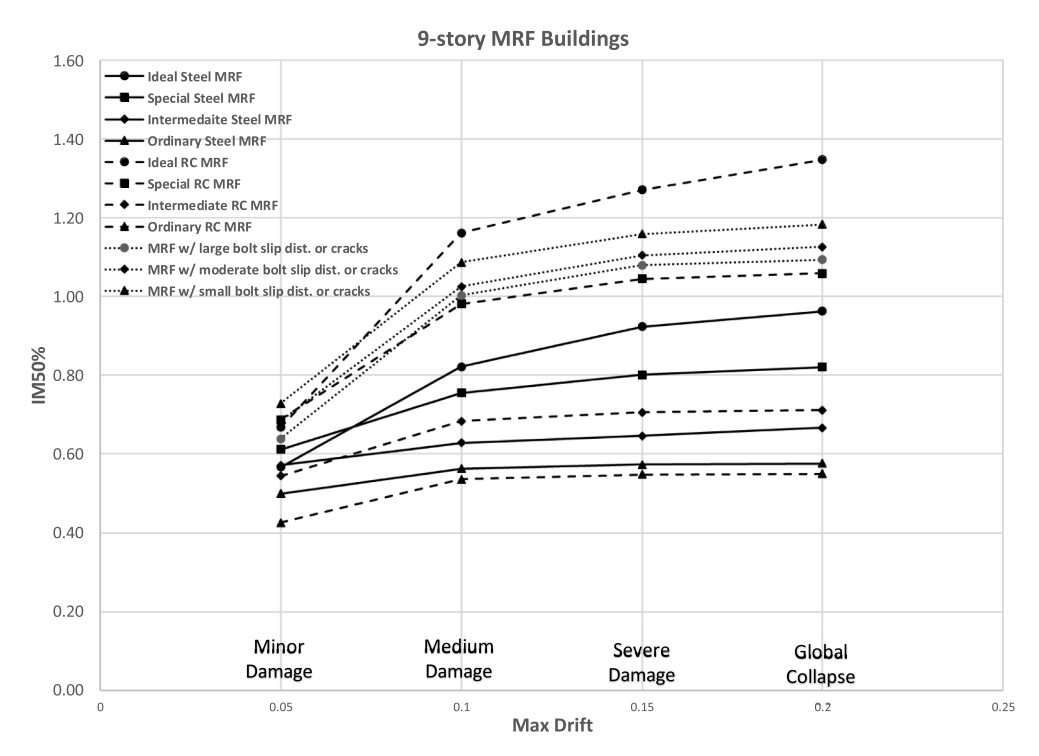


Fig. 11. IM_{50%} values of the 9-story MRF buildings.

Table 6Calculated and recommended reduction factors.

| Frames Type | Hysteresis Model | Minor LS | Medium LS | Severe LS | Collapse LS | Recommended Reduction Factor |
|----------------------|-------------------|----------|-----------|-----------|-------------|------------------------------|
| Lower-rise (3-story |) NEHRP Steel MRF | | | | | |
| C1 | 10%SD | 0.967 | 0.989 | 1.004 | 1.006 | 0.95 |
| C3 | 25%SD | 0.911 | 0.954 | 0.985 | 0.981 | 0.90 |
| C4 | 40%SD | 0.869 | 0.910 | 0.991 | 1.003 | 0.85 |
| Slip | Pinching | 0.950 | 1.021 | 1.142 | 1.300 | 0.95 |
| Lower-rise (3-story |) NEHRP RC MRF | | | | | |
| C5 | kD + 10%SD | 0.844 | 0.931 | 0.894 | 0.833 | 0.80 |
| C6 | kD + 25%SD | 0.844 | 0.810 | 0.700 | 0.624 | 0.60 |
| C7 | Kd + 40%SD | 0.759 | 0.688 | 0.632 | 0.531 | 0.50 |
| Cracked | Pinching | 0.987 | 0.963 | 0.924 | 0.922 | 0.90 |
| Mid-rise (9-story) l | NEHRP Steel MRF | | | | | |
| C1 | 10%SD | 1.078 | 0.920 | 0.867 | 0.852 | 0.85 |
| C3 | 25%SD | 1.009 | 0.765 | 0.699 | 0.692 | 0.75 |
| C4 | 40%SD | 0.881 | 0.686 | 0.620 | 0.598 | 0.60 |
| Slip | Pinching | 1.206 | 1.264 | 1.206 | 1.177 | 1.00 |
| Mid-rise (9-story) l | NEHRP RC MRF | | | | | |
| C5 | kD + 10%SD | 1.030 | 0.845 | 0.822 | 0.786 | 0.75 |
| C6 | kD + 25%SD | 0.815 | 0.589 | 0.556 | 0.528 | 0.50 |
| C7 | Kd + 40%SD | 0.638 | 0.461 | 0.431 | 0.408 | 0.40 |
| Cracked | Pinching | 1.024 | 0.894 | 0.877 | 0.842 | 0.80 |

the sample estimates, and it is known that using these to define the specific reference distribution changes the null distribution of the test statistic. Simard and L'Ecuyer [38] reported that the KS test is more powerful than the SW test because the SW test does not work well for a small sample size. Whereas, Steinskog et al. [40] pointed out that the SW test for normality is better than the KS test. Thus, both KS and SW tests were utilized in this study to doubly confirm the lognormality behaviors of these curves. The distributions were validated to be lognormal distribution. Table 5 also shows the median and logarithmic standard deviations of the curves. Using the same testing method as for the idealized 9-story steel MRF building, all other 3-story and 9-story building models were examined by normality tests. It was confirmed that all cases were lognormal probability distributions. Thus, it was feasible to use lognormal distribution to develop the fragility curves of this study.

The fragility curves of steel and RC MRF buildings for both 3-story and 9-story with different hysteresis behavior models were successfully constructed using the cumulative lognormal distribution function. When performing the cumulative lognormal regression, the probability of each damage limit state was calculated by dividing the number of earthquakes being considered. The cumulative probability was then calculated by adding all the probabilities of damage limit states from the highest damage scale to the interested damage scale, representing the probability of reaching or exceeding a damage scale at Sa (T1, -%). The cumulative probability values were then fitted with a lognormal fragility function, as shown in Eq. (2). A cumulative lognormal curve-fitting program was developed in this study to examine the efficiency and accuracy of the developed curves. The coefficient of determination R² was computed. As an example, the R2 for the data of the idealized 9-story steel MRF building are listed in Table 5. Figs. 8 and 9 show the resulted fragility curves expressing the probabilities of 3-story and 9-story MRF buildings reaching or exceeding each of the four damage limitstates, as a function of Sa (T1, -%), respectively.

6. Seismic damage safety

FEMA-P695 defines the damage margin ratio (DMR) as the safety measure of a building for an earthquake, which is a ratio of the spectral acceleration for 50% of the pre-define earthquake records causing a specific level of damages (IM $_{50\%}$) to the spectral acceleration of the max considered earthquake (MCE) ground motion (IM $_{MCE}$). The larger value of DMR implies that the building has a higher level of seismic damage safety.

Assume that all the buildings in this study were at the same locations and had the same values of IM_{MCE} . Therefore, their $IM_{50\%}$ values can

represent their seismic damage safety status. According to the fragility curves in Figs. 6 and 7, the IM $_{50\%}$ values of all buildings in this study were calculated. Fig. 10 compares the IM $_{50\%}$ values of the 3-story MRF buildings with different building hysteresis models and at different damage limit states. Fig. 11 compares the IM $_{50\%}$ values of the 9-story MRF buildings with different building hysteresis models and at different damage limit states. Based on the comparison with ideal steel and RC MRF models, Table 6 summarizes the calculated and recommended reduction factors for NEHRP MRF structures when using earthquake fragility methods and IM values, which could be helpful for building designers.

7. Conclusions

This study aimed at analyzing the hysteresis effects on the earthquake fragility curves of MRF structures and providing seismic fragility curves for various NEHRP MRF structures. The SAC prototype buildings with 3-story and 9-story MRF structures were adopted in this study to represent the lower-rise and mid-rise MRFs. Hysteresis behaviors of the beam-column joint were used in this research to describe the different behavior of different types of NEHRP MRF structures. ELEMENT 10 in the DRAIN-2DX software was adopted to model these hysteresis behaviors of the MRF joints. The fragility curves of steel and RC MRF buildings with different hysteresis behavior models were successfully constructed using the cumulative lognormal distribution function. According to the fragility curves, the earthquake damage safeties of all MRF buildings with different hysteresis models and at different damage limit states were analyzed and compared. A group of hysteresis reduction factors was proposed for modifying previous earthquake fragility analysis results of building behaviors, which can be used for building design when designers and decision-makers adopting other existing earthquake fragility curves for MRF structures. The developed fragility curves and reduction factors can also serve as a measure of assessing structure vulnerability, providing decision-makers with a better understanding of structural behavior when an earthquake occurs.

This study proposes future works, including the utilization of advanced data analytics techniques, e.g., the machine deep learning, geodatabase, and virtual information fabric such as VIFI, to explore more accurate earthquake risk assessment for all types of building structures.

CRediT authorship contribution statement

Zhenhua Huang: Supervision, Conceptualization, Methodology,

Software. **Liping Cai:** Formal analysis, Data curation, Writing - original draft. **Yashica Pandey:** Visualization. **Yong Tao:** Conceptualization, Funding acquisition. **William Telone:** Software, Funding acquisition.

Declaration of Competing Interest

The authors declare that they have no known competing financial interests or personal relationships that could have appeared to influence the work reported in this paper.

Appendix A. Supplementary material

Supplementary data to this article can be found online at https://doi.org/10.1016/j.engstruct.2021.112532.

References

- Asgarian B, Ordoubadi B. Effects of structural uncertainties on seismic performance of steel moment-resisting frames. J Constr Steel Res 2016;120:132–42. https://doi. org/10.1016/j.jcsr.2015.12.031.
- [2] Ataei N, Padgett JE. Fragility surrogate models for coastal bridges in hurricaneprone zones. Eng Struct 2015;103:203–13. https://doi.org/10.1016/j. engstruct.2015.07.002.
- [3] Bao X, Zhang MH, Zhai CH. Fragility analysis of a containment structure under farfault and near-fault seismic sequences considering post-mainshock damage states. Eng Struct 2019;198:109511. https://doi.org/10.1016/j.engstruct.2019.109511.
- [4] Calabresea A, Lai CG. Fragility functions of blockwork wharves using artificial neural networks. Soil Dyn Earthq Eng 2013;52:88–102. https://doi.org/10.1016/j. soildvn.2013.05.002.
- [5] Cha YJ, Bai JW. Seismic fragility estimates of a moment-resisting frame building controlled by MR dampers using performance-based design. Eng Struct 2016;116: 192–202. https://doi.org/10.1016/j.engstruct.2016.02.055.
- [6] Fattahi F, Gholizadeh S. Seismic fragility assessment of optimally designed steel moment frames. Eng Struct 2019;179:37–51. https://doi.org/10.1016/j. engstruct.2018.10.075.
- [7] FEMA (Federal Emergency Management Agency). Multi-hazard loss estimation methodology-Hurricane model: HAZUS-MH 2.1 Technical manual; 2012.
- [8] FEMA (Federal Emergency Management Agency), Hazards U.S. Multi-Hazard (HAZUS MH) Assessment Tool vol.3; 2011.
- [9] FEMA (Federal Emergency Management Agency), Multi-hazard loss estimation methodology-Hurricane model: HAZUS-MH-MR4 technical manual; 2009.
- [10] Gernay T, Khorasani EN, Garlock M. Fire fragility curves for steel buildings in a community context: A methodology. Eng Struct 2016;113:259–76. https://doi.org/ 10.1016/j.engstruct.2016.01.043.
- [11] Ghosh J, Padgett JE, Dueas-Osorio L. Surrogate modeling and failure surface visualization for efficient seismic vulnerability assessment of highway bridges. Probab Eng Mech 2013;34:189–99. https://doi.org/10.1016/j. probengmech.2013.09.003.
- [12] Goel R, Chopra A. Vibration properties of buildings determined from recorded earthquake motions. Report UCB/EERC-97/14, Earthquake Engineering. Berkeley, CA: Research Center University of California; 1997.
- [13] Hardyniec A, Charney F. A new efficient method for determining the collapse margin ratio using parallel computing. Comput Struct 2015;148:15–25. https://doi.org/10.1016/j.compstruc.2014.11.003.
- [14] Herbin AH, Barbato M. Fragility curves for building envelope components subject to windborne debris impact. J Wind Eng Ind Aerodyn 2012;107–108:285–98. https://doi.org/10.1016/j.iweja.2012.05.005.
- [15] Huang Z, Foutch DA. Effect of Hysteresis Type on Drift Limit for Global Collapse of Moment Frame Structures under Seismic Loads. J Earthquake Eng 2009;13: 939–64. https://doi.org/10.1080/13632460902859144.
- [16] Jeong SH, Elnashai AS. Probabilistic fragility analysis parameterized by fundamental response quantities. Eng Struct 2007;29:1238–51. https://doi.org/ 10.1016/j.engstruct.2006.06.026.
- [17] Khalfan M, El-Dakhakhni WW, Tait MJ. Seismic Risk Assessment of Nonengineered Residential Buildings in Developing Countries. J Perform Constr Facil 2016;30: 04016013. https://doi.org/10.1061/(ASCE)CF.1943-5509.0000829.
- [18] Konthesingha C, Stewart MG, Ryan PC, Ginger JD, Henderson DJ. Reliability-based vulnerability modeling of metal-clad industrial buildings to extreme wind loading for cyclonic regions. J Wind Eng Ind Aerodyn 2015;147:176–85. https://doi.org/ 10.1016/j.jweia.2015.10.002.
- [19] LaFave JM, Wight JK. Reinforced concrete wide-beam construction vs. conventional construction: resistance to lateral earthquake loads. Earthquake Spectra 2001;17(479–05). https://doi.org/10.1193/1.1586185.

- [20] Lallemant D, Kiremidjian A, Burton H. Statistical procedures for developing earthquake damage fragility curves. Earthq Eng Struct Dyn 2015;44:1373–89. https://doi.org/10.1002/eqe.2522.
- [21] Lilliefors H. On the Kolmogorov-Smirnov test for the exponential distribution with mean unknown. J Am Stat Assoc 1969;64:387–9.
- [22] Luco N, Cornell CA. Effects of connection fractures on SMRF seismic drift demands. ASCE J Struct Eng 2000;126:127–36. https://doi.org/10.1061/(ASCE)0733-9445 (2000)126:1(127).
- [23] Macabuag J, Rossetto T, Ioannou I, EamesI I. Investigation of the Effect of Debris-Induced Damage for Constructing Tsunami Fragility Curves for Buildings. Geosciences 2018;8(4):117. https://doi.org/10.3390/geosciences8040117.
- [24] Maloney T, Ellingwood B, Mahmoud H, Wang N, Wang Y, Lin P. Performance and risk to light-framed wood residential buildings subjected to tornadoes. Struct Saf 2018;70:35–47. https://doi.org/10.1016/j.strusafe.2017.10.004.
- [25] Medina S, Lizarazo-Marriaga J, Estrada M, Koshimura S, Mas E, Adriano B. Tsunami analytical fragility curves for the Colombian Pacific coast: A reinforced concrete building example. Eng Struct 2019;196:109309. https://doi.org/ 10.1016/j.engstruct.2019.109309.
- [26] Mishra S, Vanli OA, Alduse BP, Jung S. Hurricane loss estimation in wood-frame buildings using Bayesian model updating: Assessing uncertainty in fragility and reliability analyses. Eng Struct 2017;135:81–94. https://doi.org/10.1016/j. engstruct.2016.12.063.
- [27] Mitropoulou CC, Papadrakakis M. Developing fragility curves based on neural network IDA predictions. Eng Struct 2011;33:3409–21. https://doi.org/10.1016/j. engstruct 2011/07/005
- [28] Noh HY, Lallemant D, Kiremidjian AS. Development of empirical and analytical fragility functions using kernel smoothing methods. Earthq Eng Struct Dyn 2015; 44:1163–80. https://doi.org/10.1002/eqe.2505.
- [29] Pitilakis KD, Karapetrou ST, Fotopoulou SD. Consideration of aging and SSI effects on seismic vulnerability assessment of RC buildings. Bull Earthq Eng 2014;12: 1755–76. https://doi.org/10.1007/s10518-013-9575-8.
- [30] Prakash V, Powell GH, Campbell S. DRAIN-2DX Element Description and User Guide. Berkeley: University of California Press: 1993.
- [31] Rehman K, Cho YS. Building Damage Assessment Using Scenario-Based Tsunami Numerical Analysis and Fragility Curves. WATER 2016;8:109–26. https://doi.org/ 10.3390/w8030109.
- [32] Rossetto T, Elnashai AS. Derivation of vulnerability functions for European-type RC structures based on observational data. Eng Struct 2003;25:1241–63. https://doi. org/10.1016/S0141-0296(03)00060-9.
- [33] SAC-96-02. Connection Test Summaries (available through Applied Technology Council); 1996.
- [34] Schneider SP, Teeraparbwong I. Bolted Flange Plate Connections. Report SAC/BD-00/05 (available from Applied Technology Council); 2000.
- [35] Shafei B, Zareian F, Lignos DG. A simplified method for collapse capacity assessment of moment resisting frame and shear wall structural systems. Eng Struct 2011;33:1107–16. https://DOI:10.1016/j.engstruct.2010.12.028.
- [36] Shi S, Foutch DA. Evaluation of Connection Fracture and Hysteresis Type on the Seismic Response of Steel Buildings. Ph.D. Thesis. Urbana, IL: University of Illinois at Urbana-Champaign; 1997.
- [37] Shin M, LaFave JM. Seismic performance of reinforced concrete eccentric beamcolumn connections with floor slabs. ACI Struct J 2004;101:403–12.
- [38] Simard R, L'Ecuyer P. Computing the Two-Sided Kolmogorov-Smirnov Distribution". J Stat Softw 2011;39(11):1–18. https://doi.org/10.18637/jss.v039. i11
- [39] Somerville P, Smith N, Puntamurthula S, Sun J. Development of ground motion time histories for phase 2 of the FEMA/ SAC steel project. In: SAC Background Document SAC/BD-97/04, SAC Joint Venture, Richmond, Calif; 1997.
- [40] Steinskog DJ, Tjøstheim DB, Kvamstø NG. A Cautionary Note on the Use of the Kolmogorov-Smirnov Test for Normality. Mon Weather Rev 2007;135(3):1151–7. https://doi.org/10.1175/MWR3326.1.
- [41] Stewart MG, Ryan PC, Henderson DJ, Ginger JD. Fragility analysis of roof damage to industrial buildings subject to extreme wind loading in non-cyclonic regions. Eng Struct 2016;128:333–43. https://doi.org/10.1016/j.engstruct.2016.09.053.
- [42] Takeda T, Sozen MA, Nielsen NN. Reinforced Concrete Response to Simulated Earthquake. ASCE J Struct Div 1970;96:2557–73.
- [43] Veneziano D, Casciati F, Faravelli L. Method OP Seismic Fragility for Complicated Systems. Probabilistic Methods in Seismic Risk Assessment for Nuclear Power Plants; 1983.
- [44] Wang Z, Pedroni N, Zentner I, Zioc E. Seismic fragility analysis with artificial neural networks: Application to nuclear power plant equipment. Eng Struct 2018; 162:213–25. https://doi.org/10.1016/j.engstruct.2018.02.024.
- [45] Yun SY, Hamburger RO, Cornell CA, Foutch DA. Seismic Performance Evaluation for Steel Moment Frames. J Struct Eng 2002;April:534–45. https://doi.org/ 10.1061/(ASCE)0733-9445(2002)128:4(534).
- [46] Yun S, Foutch DA. Performance Prediction and Evaluation of Loe Ductility Steel Moment Frame for Seismic Loads. SAC Background Report SAC/BD-00/26, SAC Joint Venture; 2000.
- [47] Zentner I, Gündel M, Bonfils N. Fragility analysis methods: a review of existing approaches and application. Nucl Eng Des 2017;323:245–58. https://doi.org/ 10.1016/j.nucengdes.2016.12.021.